Journal of Materials Chemistry C

PAPER

View Article Online
View Journal | View Issue

Cite this: J. Mater. Chem. C, 2019, 7, 330

Robust luminescent small molecules with aggregation-induced delayed fluorescence for efficient solution-processed OLEDs†

Jian Huang,‡[a] Zeng Xu,‡[a] Zheyi Cai,[a] Jingjing Guo,[a] Jiali Guo,[a] Pingchuan Shen,[a] Zhiming Wang,[a] Zujin Zhao,*[a] Dongge Ma*[a] and Ben Zhong Tang*[ab]

Purely organic luminescent materials with thermally activated delayed fluorescence have the merits of high exciton utilization and thus excellent electroluminescence (EL) efficiency in OLEDs. However, these devices, particularly solution-processed doped OLEDs, usually encounter the troublesome problem of severe efficiency roll-off at high voltages. Herein, two new organic small molecules consisting of electron-withdrawing benzoyl and electron-donating 9-hexylcarbazole and phenoxazine (or 9,9-dimethyl-9,10-dihydroacridine) moieties are designed and synthesized. The crystal and electronic structures, thermal stabilities, electrochemical behaviors and photophysical properties are thoroughly investigated. Whereas these materials are weak emitters in solution, they can fluoresce strongly in spin-coated neat films with greatly enhanced delayed fluorescence, namely they possess interesting aggregation-induced delayed fluorescence (AIDF). Solution-processed nondoped OLEDs are fabricated by using these materials as light-emitting layers, which provide high EL efficiencies of up to 9.02%. Efficient doped OLEDs with varied doping concentrations (10, 30 and 50 wt%) in a 4,4′-bis(carbazol-9-yl)biphenyl (CBP) host are also obtained by a spin-coating technique, offering higher EL efficiencies of up to 12.1%. More importantly, both solution-processed nondoped and doped OLEDs exhibit an extremely small efficiency roll-off (down to 0.08% at 1000 cd m^{-2} luminance), demonstrating the greatly advanced efficiency stability. These results clearly prove that luminescent materials with AIDF properties are promising candidates for the fabrication of high-performance solution-processed OLEDs.

Received 25th September 2018,
Accepted 29th November 2018

DOI: 10.1039/c8tc04842h

rsc.li/materials-c

Introduction

As a promising display and lighting technique, organic light-emitting diodes (OLEDs) have drawn intense interest from academia and industry. To realize massive commercialization, highly efficient and low-cost light-emitting materials are of crucial importance. However, most luminescent materials are unable to function efficiently in OLEDs because of aggregation-caused emission quenching and exciton annihilation. For example, purely organic materials with thermally activated delayed fluorescence (TADF) have the merits of high exciton utilization and low cost.[1,2] They usually have small singlet–triplet energy splitting (ΔE_{ST}), and the up-conversion of non-radiative triplet excitons (75%) to radiative singlet ones is promoted *via* a reverse intersystem crossing (RISC) process under thermal activation, theoretically endowing electroluminescence (EL) devices with 100% internal quantum efficiency.[3,4] Due to the long lifetimes of triplet excited states, conventional TADF emitters have to be dispersed within appropriate hosts to suppress concentration-caused exciton annihilation. However, at high voltages, this doping technique becomes invalid because of the too high exciton density for most OLEDs based on TADF emitters. Eventually, the EL efficiency decreases dramatically due to serious bimolecular quenching processes, such as triplet–triplet annihilation (TTA) and singlet–triplet annihilation (STA).[5] To solve this problem, we recently developed a series of novel luminogenic molecules with aggregation-induced delayed fluorescence (AIDF).[6,7] They are free of aggregation-caused quenching and can fully harness both singlet and triplet excitons in nondoped OLEDs without serious high-concentration exciton

[a] State Key Laboratory of Luminescent Materials and Devices, Center for Aggregation-Induced Emission, South China University of Technology, Guangzhou 510640, China. E-mail: mszjzhao@scut.edu.cn, msdgma@scut.edu.cn
[b] Department of Chemistry, Hong Kong Branch of Chinese National Engineering Research Center for Tissue Restoration and Reconstruction, The Hong Kong University of Science and Technology, Clear Water Bay, Kowloon, Hong Kong, China. E-mail: tangbenz@ust.hk

† Electronic supplementary information (ESI) available: TGA and DSC thermograms, fluorescence and phosphorescence spectra, and photophysical parameters. CCDC 1838714. For ESI and crystallographic data in CIF or other electronic format see DOI: 10.1039/c8tc04842h

‡ J. H. and Z. X. contributed equally to this work.

annihilation at high luminance, demonstrating great potential for the fabrication of high-performance OLEDs with advanced EL efficiencies and stabilities.[6b–d]

In comparison with vacuum deposition, solution-processed film preparation techniques, including spin-coating, inkjet printing, roll to roll processing, *etc.*, are more feasible to manufacture large-area OLEDs with less material waste and reduced cost.[8] Moreover, flexible substrates and better control of the doping process can be facilely adopted. Currently, the majority of light-emitting materials used in solution-processed OLEDs are luminescent polymers, including the emerging TADF polymers,[9,10] because of their good film-forming ability. However, the low reproducibility, metal catalyst residue, and structural defects of luminescent polymers will undermine their EL performance. In contrast, small molecules have the merits of clearly defined structures, easy purification and better photoluminescence (PL) efficiencies. Besides fluorescent and phosphorescent small molecules,[11,12] there is a considerable interest focused on the development of solution-processable small molecules with TADF properties.[13,14] Although inspiring achievements have been made, their OLEDs fabricated by solution-process techniques still often encounter the troublesome problem of sharp efficiency loss at high voltages, just like most vacuum-deposited TADF emitters. To address this issue, in this contribution, we designed and synthesized two new small molecules possessing AIDF, with long alkyl chains to increase their film-forming ability during the solution-processing technique. They emit bright green and yellow light with evident delayed fluorescence in spin-coated films. The solution-processed nondoped and doped OLEDs are fabricated using both small molecules, which provide high EL efficiencies and an extremely small efficiency roll-off.

Results and discussion

Synthesis

The synthesis of target compounds CC6-DBP-PXZ and CC6-DBP-DMAC is simple and efficient. As shown in Scheme 1, 9-hexylcarbazole (**1**) prepared by a literature method underwent Friedel–Crafts acylation reaction with compound **2** to yield intermediate **3**. The treatment of **3** with phenoxazine (PXZ, **4a**) and 9,9-dimethyl-9,10-dihydroacridine (DMAC, **4b**) furnished CC6-DBP-PXZ and CC6-DBP-PXZ, respectively. The molecular structures were well characterized by NMR and high-resolution mass spectra. Owing to the presence of hexyl groups, both compounds have good solubility in common organic solvents, such as chlorobenzene, toluene, chloroform, dichloromethane, tetrahydrofuran (THF), and so forth, but are hardly soluble in water because of their hydrophobic nature.

Single crystal structure

Single crystals of CC6-DBP-PXZ were obtained from a methanol–dichloromethane mixture by slow solvent evaporation. The crystal structure of CC6-DBP-PXZ shows a twisted conformation, in which the electron-donating PXZ units are connected with phenyl rings at the 9-positions in an almost vertical manner (Fig. 1). The torsion angles between them are as large as 81.1° and 89.3°. Such a twisted conformation is favorable for the separation of frontier orbitals and thus a small ΔE_{ST} of the molecule. Generally, CC6-DBP-PXZ molecules are packed in a loose pattern because of the twisted conformation. But, one of the peripherical PXZ units in CC6-DBP-PXZ can align nearly parallel and face-to-face to a neighouring PXZ with an inter-ring distance of 3.320 Å, indicative of a π–π stacking interaction. There are also multiple weak intermolecular interactions, such as C–H···π hydrogen bonds (2.755 and 2.858 Å), formed amongst CC6-DBP-PXZ molecules. These interactions can help to restrict intramolecular motions and rigidify molecular structures.[15]

Thermal stabilities

The thermal stability of both compounds was evaluated by thermogravimetric analysis (TGA) and differential scanning calorimetry (DSC) under nitrogen. CC6-BP-PXZ and CC6-BP-DMAC show high decomposition temperatures of 475 and 438 °C, and high glass-transition temperatures of 114.3 and 120.4 °C, respectively (Fig. S1, ESI†). The excellent thermal and morphological stabilities of both compounds meet the requirements of solution-proceeded OLEDs, and benefit device performance.

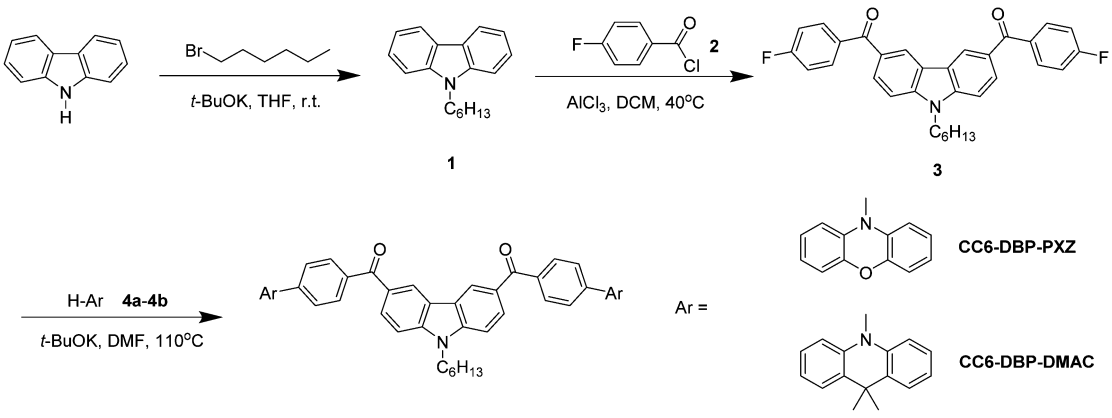

Scheme 1 Synthetic routes of CC6-DBP-PXZ and CC6-DBP-DMAC. DCM = dichloromethane; DMF = *N*,*N*-dimethylformamide.

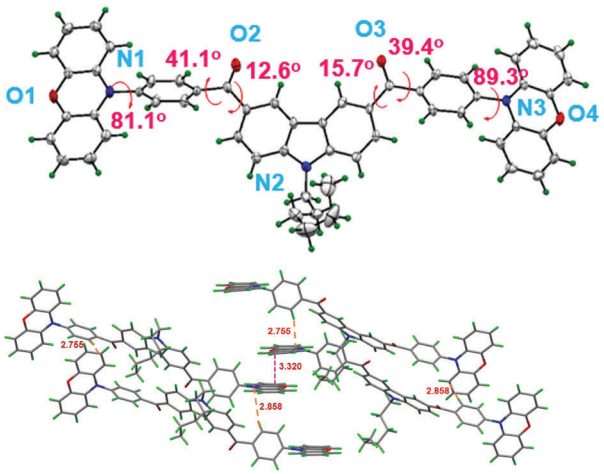

Fig. 1 Crystal structure of CC6-DBP-PXZ with thermal ellipsoids set at 50% probability. Molecular packing of CC6-DBP-PXZ in the crystal with indicated distances (Å) of π–π stacking interactions and C–H···π hydrogen bonds.

Photophysical behaviours

In dilute THF solutions, CC6-DBP-PXZ and CC6-DBP-DMAC show absorption maxima at ~335 and ~343 nm, respectively, which are associated with the π–π* transition of the molecules. Meanwhile, weak absorption tails extending to ~445 nm are observed (Fig. 2A), owing to the twisted intramolecular charge transfer (TICT) from the electronic donating–accepting (D–A) structure. This absorption tail of CC6-DBP-PXZ is relatively stronger than that of CC6-DBP-DMAC because of the stronger electron-donating ability of PXZ than DMAC. CC6-DBP-PXZ and CC6-DBP-DMAC emit weakly at 582 and 525 nm, with a low fluorescence quantum yield (Φ_F) of 4.1% and 11.7%, respectively. However, in neat films, they show strong blue-shifted emissions at 547 and 510 nm, respectively (Fig. 2B). The blue-shifted emissions from THF solutions to neat films are attributed to the decreased polarity of the environment, in which a single fluorogenic molecule experiences a weakened TICT effect. The Φ_F values of CC6-DBP-PXZ and CC6-DBP-DMAC are greatly increased to 38.3% and 59.5%, respectively, indicating that both compounds behave better in solid form than in solution as light-emitting materials. To further confirm this, the emission behaviors of both compounds in THF–water mixtures were measured. It can be seen that their aggregates formed in the mixtures with high water fractions show blue-shifted and stronger emissions relative to those in THF solutions (Fig. 2C and D). This finding is in good agreement with the emission properties in their neat films. The enhanced emissions of the aggregates and neat films are attributed to the restriction of intramolecular motions, and thus the blocking of nonradiative decay of the excited state.[16]

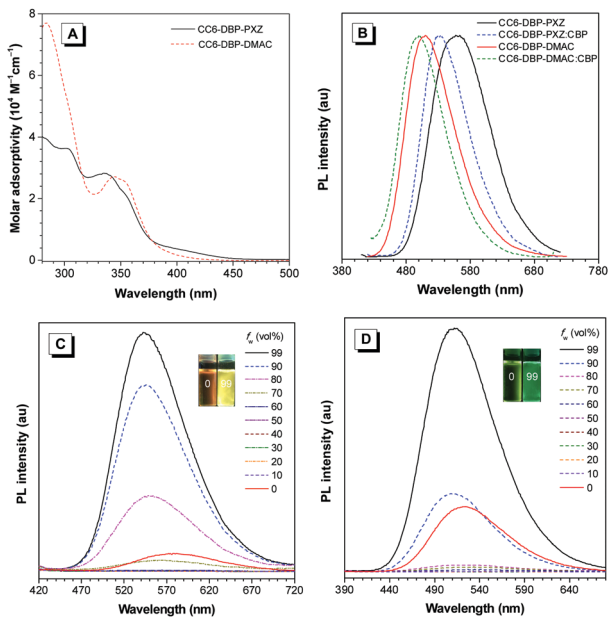

Fig. 2 (A) Absorption spectra in THF solutions (10^{-5} M) and (B) PL spectra in neat films and doped films in the CBP matrix (30 wt%) of CC6-DBP-PXZ and CC6-DBP-DMAC. PL spectra of (C) CC6-DBP-PXZ and (D) CC6-DBP-DMAC in THF–water mixtures with different water fractions (f_w). Insets in (C) and (D): photos of compounds in THF–water mixtures (f_w = 0 and 99%), taken under the illumination of a UV lamp (365 nm).

The transient PL decay spectrum shows that CC6-DBP-PXZ has a short lifetime of 2.0 ns, and the delayed fluorescence is hardly observed in solution (Table S1, ESI†). CC6-DBP-DMAC shows a longer lifetime of 60.7 ns, and the lifetimes of prompt fluorescence and delayed fluorescence are 19.7 ns and 217.2 ns, with ratios of 79% and 21%, respectively. In comparison with CC6-DBP-PXZ, the delayed fluorescence of CC6-DBP-DMAC is more obvious, which is probably due to the relatively more rigid structure of DMAC than that of PXZ. The neat films of CC6-DBP-PXZ and CC6-DBP-DMAC show much longer mean lifetimes of 0.24 and 1.29 μs, with prompt fluorescence lifetimes of 22.9 and 25.7 ns and apparent delayed fluorescence lifetimes of 1.2 and 2.9 μs, respectively (Table 1 and Table S2, ESI†). These results indicate that the delayed fluorescence of both compounds is more likely to occur in films than in solutions (Fig. 3A and B), clearly demonstrating the AIDF nature.[6,17] The ΔE_{ST} values of the neat films of CC6-DBP-PXZ and CC6-DBP-DMAC were measured to be 0.02 and 0.04 eV, respectively, from their fluorescence and phosphorescence spectra (Fig. S2, ESI†). These values are small enough for the occurrence of RISC and thus delayed fluorescence at room temperature. To further validate the delayed fluorescence, the temperature dependence of the transient PL decay spectra was investigated. As shown in Fig. 3C and D, the lifetime of delayed fluorescence is elongated and the ratio of the delayed component increased with the increase of temperature. This is the distinctive character of delayed fluorescence because the high temperature can promote the RISC process. These results demonstrate that both compounds have more efficient emissions with enhanced delayed fluorescence in neat films than in solutions. But, for CC6-DBP-DMAC, the changes of the transient PL decay curves are somewhat complicated below 300 K, which is probably due to the presence of phosphorescence, namely the coexistence of phosphorescence, delayed fluorescence and prompt fluorescence.

Table 1 Photophysical properties of CC6-DBP-PXZ and CC6-DBP-DMAC

	Soln[a]			Neat film[b]					Doped film[c]				
	λ_{abs} (nm)	λ_{em} (nm)	Φ_F[d] (%)	λ_{em} (nm)	Φ_F[d] (%)	τ_{prompt}[e] (ns)	$\tau_{delayed}$[e] (μs)	ΔE_{ST}[f] (eV)	λ_{em} (nm)	Φ_F[d] (%)	τ_{prompt}[e] (ns)	$\tau_{delayed}$[e] (μs)	ΔE_{ST}[f] (eV)
CC6-DBP-PXZ	335	582	4.1	547	38.3	22.9	1.2	0.02	531	59.0	24.5	1.6	0.07
CC6-DBP-DMAC	343	525	11.7	510	59.5	25.7	2.9	0.04	500	69.1	29.4	6.4	0.05

[a] In THF solution (10^{-5} M) at room temperature. [b] Spin-coated on a quartz substrate. [c] Spin-coated doped film in CBP at a concentration of 30 wt%. [d] Absolute fluorescence quantum yield determined by a calibrated integrating sphere under nitrogen at room temperature. [e] PL lifetimes of prompt (τ_{prompt}) and delayed ($\tau_{delayed}$) decay components evaluated at 300 K under vacuum. [f] Estimated from the high-energy onsets of fluorescence and phosphorescence spectra at 77 K.

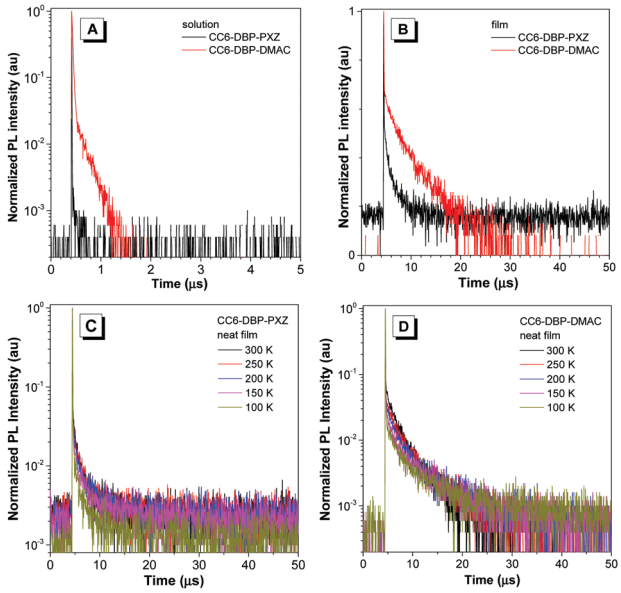

Fig. 3 Transient PL decay spectra of CC6-DBP-PXZ and CC6-DBP-DMAC (A) in THF solutions (10^{-5} M) and (B) in neat films, measured at 300 K under nitrogen. Temperature dependent transient PL decay spectra of (C) CC6-DBP-PXZ and (D) CC6-DBP-DMAC in neat films under nitrogen.

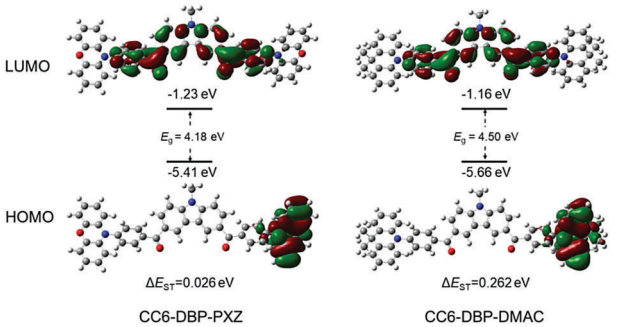

Fig. 4 Optimized molecular structures and frontier orbital amplitude plots of CC6-DBP-PXZ and CC6-DBP-DMAC, calculated by the M06-2X hybrid functional at the basis set level of 6-31G*. Hexyl was replaced with methyl for easy processing.

Theoretical calculations

DFT/TDDFT calculation was conducted to investigate the molecular orbital amplitude plots and energy levels of the highest occupied molecular orbitals (HOMOs) and the lowest unoccupied molecular orbitals (LUMOs) of both compounds. As shown in Fig. 4, the HOMO of CC6-DBP-PXZ is mainly located on one of the electron-donating PXZ units, while the LUMOs are on the electron-withdrawing benzoyl as well as electron-donating carbazole units. A similar phenomenon is observed for CC6-DBP-DMAC. Clearly, the distributions of HOMOs and LUMOs are well separated in both compounds, which is favorable to achieve a small ΔE_{ST} as well as the occurrence of the TICT process. Indeed, the calculated ΔE_{ST} values are 0.026 and 0.262 eV for CC6-DBP-PXZ and CC6-DBP-DMAC, respectively, which are theoretically small enough for RISC and delayed fluorescence. On the other hand, the calculated energy gap between the HOMO and LUMO of CC6-DBP-PXZ is smaller than that of CC6-DBP-DMAC, which is consistent with the red-shifted experimental absorption and emission spectra of CC6-DBP-PXZ relative to CC6-DBP-DMAC.

Electrochemical properties

The electrochemical behaviors of CC6-BP-PXZ and CC6-BP-DMAC were investigated by cyclic voltammetry (CV). Cyclic voltammograms were measured in a solution of tetra-*n*-butylammonium hexafluorophosphate (Bu_4NPF_6, 0.1 M) in acetonitrile. A three-electrode system (Ag/Ag^+, platinum wire and glassy carbon electrodes as reference, counter and working electrodes, respectively) was used at a scan rate of 100 mV s^{-1} in the measurement. As illustrated in Fig. 5, both compounds exhibit reversible oxidation and reduction processes, indicative of good electrochemical stability. The oxidation peaks of CC6-BP-PXZ and CC6-BP-DMAC are located at 0.80 and 0.62 V, respectively, and the reduction peaks are at −2.18 and −2.19 V, respectively. The HOMO energy levels of CC6-BP-PXZ and CC6-BP-DMAC were calculated to be −5.24 and −5.04 eV, respectively, from the onset oxidation potentials, and the LUMO energy levels were found to be −2.70 and −2.71 eV, respectively, from the onset reduction potentials (HOMO = $-[E_{ox} + 4.8]$ eV, and LUMO = $-[E_{re} + 4.8]$ eV,[18] where E_{ox} and E_{re} represent onset oxidation and reduction potentials relative to Fc/Fc^+, respectively).

Electroluminescence

Based on the excellent PL properties of CC6-DBP-PXZ and CC6-DBP-DMAC, we further evaluated their EL performances in solution-processed OLEDs. The nondoped OLEDs with a configuration of ITO/PEDOT:PSS (50 nm)/PVK (30 nm)/emitter/TmPyPB (40 nm)/LiF (1 nm)/Al (Device 1A: emitter = CC6-DBP-DMAC (65 nm);

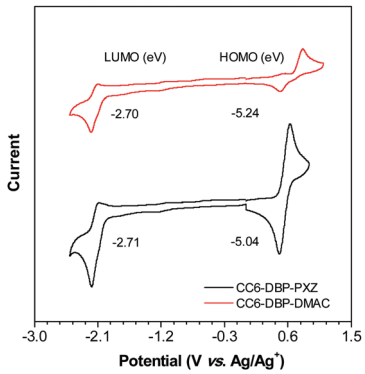

Fig. 5 Cyclic voltammograms of CC6-DBP-PXZ and CC6-DBP-DMAC measured in acetonitrile containing 0.1 M tetra-*n*-butylammonium hexafluorophosphate. Scan rate: 100 mV s^{-1}.

Device 1B: emitter = CC6-DBP-DMAC (60 nm); Device 1C: emitter = CC6-DBP-PXZ (40 nm); Device 1D: emitter = CC6-DBP-PXZ (60 nm)) were fabricated, in which poly(3,4-ethylenedioxythiophene):poly(styrenesulfonate) (PEDOT:PSS) and LiF were used as hole- and electron-injecting layers, respectively; poly(9-vinylcarbazole) (PVK) and 1,3,5-tri(*m*-pyrid-3-yl-phenyl)-benzene (TmPyPB) were selected for the hole- and electron-transporting layers, respectively. The neat films of CC6-DBP-PXZ and CC6-DBP-DMAC prepared by spin-coating served as the light-emitting layers. The key EL data of the nondoped devices are summarized in Table 2, and the characteristic curves are displayed in Fig. 6. CC6-DBP-DMAC-based Devices 1A and 1B show turn-on voltages of 4.2 V, and radiate green light at 507 nm ($CIE_{x,y}$ = 0.272, 0.503) and 505 nm ($CIE_{x,y}$ = 0.265, 0.501), respectively. The maximum luminance (L_{max}), current efficiency ($\eta_{C,max}$), power efficiency ($\eta_{P,max}$) and external quantum efficiency ($\eta_{ext,max}$) of Device 1B are 14 366 cd m^{-2}, 25.08 cd A^{-1}, 11.25 lm W^{-1} and 9.02%, respectively. Device 1A shows similar EL performances to Device 1B. CC6-DBP-PXZ-based Devices 1C and 1D can be turned on at a lower voltage of 2.9 V, and they exhibit intense yellow light at 568 nm ($CIE_{x,y}$ = 0.454, 0.523) and 566 nm ($CIE_{x,y}$ = 0.459, 0.518) with a higher L_{max} of 30 644 and 30 626 cd m^{-2}, respectively. High $\eta_{C,max}$, $\eta_{P,max}$ and $\eta_{ext,max}$ values of 22.23 cd A^{-1}, 16.11 lm W^{-1} and 7.73%, respectively, are achieved in Device 1C. The performance of Device 1D is also similar to that of Device 1C, even if the thickness of CC6-DBP-PXZ was changed greatly. According to the photophysical parameters, the exciton utilization of these nondoped OLEDs approached nearly 100% (Table S3, ESI†). Impressively, these nondoped OLEDs show superior efficiency stability, with negligible efficiency roll-off at the luminance of 1000 cd m^{-2}. Even at 5000 cd m^{-2} luminance, the current efficiency roll-off is still very small (2.8–9.6%), which is much better than those of most solution-processed OLEDs based on TADF emitters.[13,14]

To investigate the potential of both compounds in doped OLEDs, we selected 4,4′-bis(carbazol-9-yl)biphenyl (CBP) as a

Table 2 EL performances of nondoped OLEDs based on CC6-DBP-PXZ and CC6-DBP-DMAC[a]

			Maximum values				Values at 5000 cd m^{-2}					
Device		V_{on} (V)	η_C (cd A^{-1})	η_P (lm W^{-1})	η_{ext} (%)	L (cd m^{-2})	η_C (cd A^{-1})	η_P (lm W^{-1})	η_{ext} (%)	RO (%)	λ_{EL} (nm)	CIE (x, y)
CC6-DBP-DMAC	1A	4.2	23.12	9.69	8.42	13 067	21.04	7.59	7.67	8.9	507	(0.272, 0.503)
	1B	4.2	25.08	11.25	9.02	14 366	22.65	8.83	8.15	9.6	505	(0.265, 0.501)
CC6-DBP-PXZ	1C	2.9	22.23	16.11	7.73	30 644	21.20	9.84	7.36	4.8	568	(0.454, 0.523)
	1D	2.9	20.32	15.27	7.24	30 626	19.73	8.57	7.04	2.8	566	(0.459, 0.518)

[a] Abbreviations: V_{on} = turn-on voltage at 1 cd m^{-2}; η_c = current efficiency; η_p = power efficiency; η_{ext} = external quantum efficiency; RO = current efficiency roll-off from maximum value to that at 5000 cd m^{-2}; λ_{EL} = electroluminescence maximum; CIE = Commission Internationale de I'Eclairage coordinates.

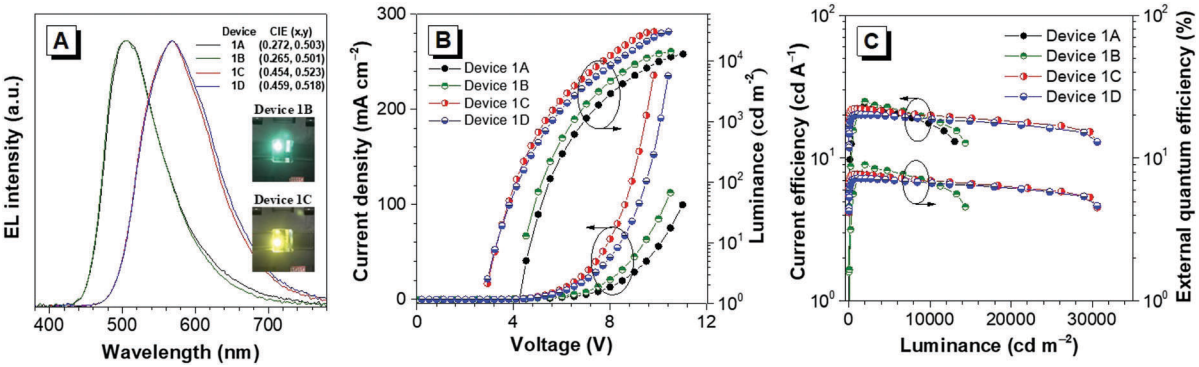

Fig. 6 (A) EL spectra, and (B) luminance–voltage–current density and (C) current efficiency–luminance–external quantum efficiency characteristics of the nondoped devices. Configurations: ITO/PEDOT:PSS (50 nm)/PVK (30 nm)/emitter/TmPyPB (40 nm)/LiF (1 nm)/Al; emitter = CC6-DBP-DMAC (65 nm) (Device 1A); emitter = CC6-DBP-DMAC (60 nm) (Device 1B); emitter = CC6-DBP-PXZ (40 nm) (Device 1C); emitter = CC6-DBP-PXZ (60 nm) (Device 1D). Insets in (A): photographs of Devices 1B and 1C.

Table 3 EL performances of doped OLEDs based on CC6-DBP-PXZ and CC6-DBP-DMAC[a]

Device		V_{on} (V)	Maximum values				Values at 1000 cd m^{-2}					
			η_C (cd A^{-1})	η_P (lm W^{-1})	η_{ext} (%)	L (cd m^{-2})	η_C (cd A^{-1})	η_P (lm W^{-1})	η_{ext} (%)	RO (%)	λ_{EL} (nm)	CIE (x, y)
CC6-DBP-DMAC	2A	4.8	20.53	8.60	8.23	9068	19.42	7.90	7.78	5.5	490	(0.201, 0.426)
	2B	3.7	27.07	14.73	10.03	11 247	25.87	12.17	9.58	4.5	499	(0.224, 0.483)
	2C	3.8	23.98	12.39	8.67	13 620	23.93	11.58	8.65	0.2	503	(0.235, 0.499)
CC6-DBP-PXZ	3A	4.0	37.62	17.76	12.13	33 286	37.57	15.51	12.12	0.08	524	(0.345, 0.560)
	3B	3.7	31.00	16.10	10.07	36 057	30.37	13.09	9.87	2.0	535	(0.383, 0.561)
	3C	3.4	28.07	14.11	9.30	32 151	27.82	13.45	9.22	0.9	540	(0.407, 0.553)

[a] Abbreviations: V_{on} = turn-on voltage at 1 cd m^{-2}; η_c = current efficiency; η_p = power efficiency; η_{ext} = external quantum efficiency; RO = current efficiency roll-off from maximum value to that at 1000 cd m^{-2}; λ_{EL} = electroluminescence maximum; CIE = Commission Internationale de l'Eclairage coordinates.

host for CC6-DBP-PXZ and CC6-DBP-DMAC to fabricate doped films at varied concentrations of 10, 30 and 50 wt%. The photophysical properties of the doped films at 30 wt% concentration were measured as an example. The emission peaks of CC6-DBP-PXZ and CC6-DBP-DMAC in the doped films are located at 531 and 500 nm with high Φ_F values of 59.0% and 69.1%, respectively. Both compounds in the doped films also show a small ΔE_{ST} and apparent delayed fluorescence (Table 1). For example, the delayed fluorescence lifetimes of CC6-DBP-PXZ and CC6-DBP-DCMA in CBP are 1.6 and 6.4 μs, which are slightly longer than those in the neat films, suggesting that a similar AIDF effect can occur in doped films as well (Table S2, ESI†).

Based on these results, we also fabricated the doped devices with a configuration of ITO/PEDOT:PSS (50 nm)/PVK (30 nm)/emitter/TmPyPB (40 nm)/LiF (1 nm)/Al (Device 2A: emitter = 10 wt% CC6-DBP-DMAC: CBP (50 nm); Device 2B: emitter = 30 wt% CC6-DBP-DMAC: CBP (55 nm); Device 2C: emitter = 50 wt% CC6-DBP-DMAC: CBP (60 nm); Device 3A: emitter = 10 wt% CC6-DBP-PXZ: CBP (50 nm); Device 3B: emitter = 30 wt% CC6-DBP-PXZ: CBP (55 nm); Device 3C: emitter = 50 wt% CC6-DBP-PXZ: CBP (60 nm)). The key EL data of the doped devices are shown in Table 3, and the characteristic curves are displayed in Fig. 7. CC6-DBP-DMAC-based doped devices show low turn-on voltages of 3.7–4.8 V, and

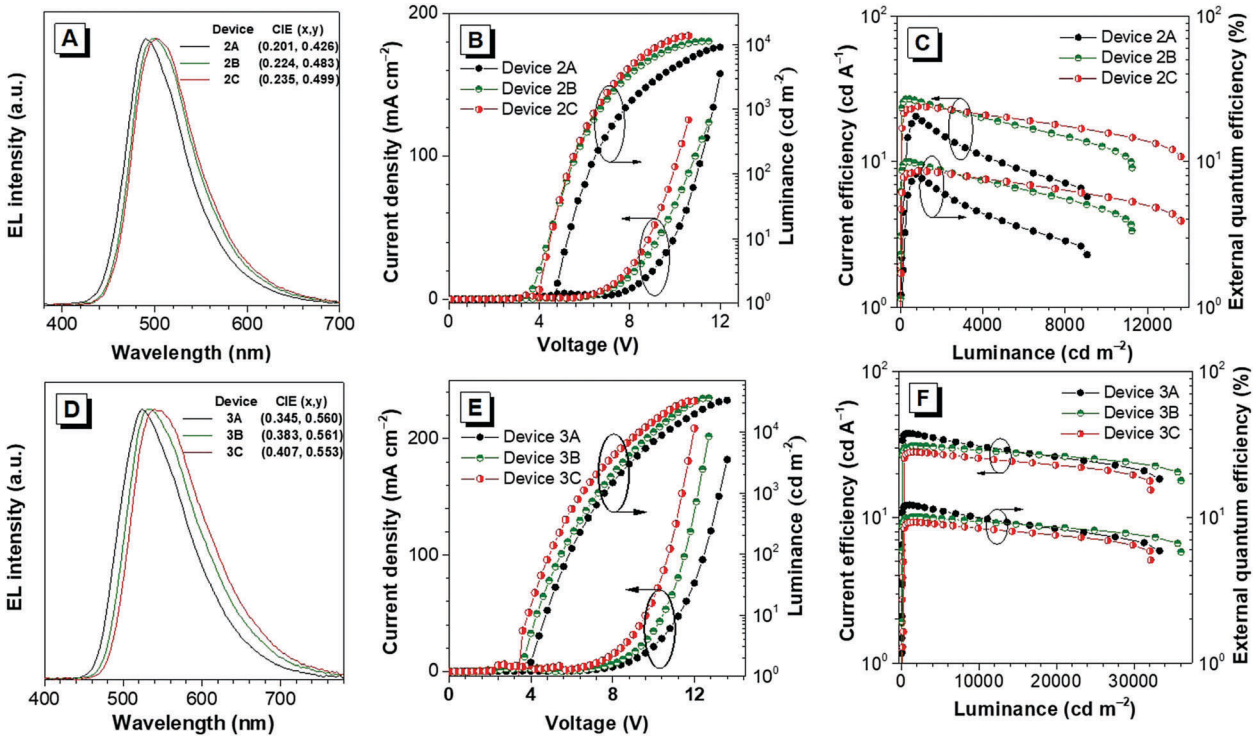

Fig. 7 (A and D) EL spectra, (B and E) luminance–voltage–current density and (C and F) current efficiency–luminance–external quantum efficiency characteristics of the doped devices. Configurations: ITO/PEDOT:PSS (50 nm)/PVK (30 nm)/emitter/TmPyPB (40 nm)/LiF (1 nm)/Al; emitter = 10 wt% CC6-DBP-DMAC: CBP (50 nm) (Device 2A); emitter = 30 wt% CC6-DBP-DMAC: CBP (55 nm) (Device 2B); emitter = 50 wt% CC6-DBP-DMAC: CBP (60 nm) (Device 2C); emitter = 10 wt% CC6-DBP-PXZ: CBP (50 nm) (Device 3A); emitter = 30 wt% CC6-DBP-PXZ: CBP (55 nm) (Device 3B); emitter = 50 wt% CC6-DBP-PXZ: CBP (60 nm) (Device 3C).

exhibit green light at 490–503 nm, slightly blue-shifted in comparison with those of the nondoped devices. Device 1B with a light-emitting layer of 30 wt% CC6-BP-DMAC doped in the CBP host shows the best EL performance with $\eta_{C,max}$, $\eta_{P,max}$, and $\eta_{ext,max}$ values of 27.1 cd A^{-1}, 14.7 lm W^{-1} and 10.0%, respectively, which are comparable to those of the nondoped devices. CC6-DBP-PXZ-based doped devices show turn-on voltages of 3.4–4.0 V, and radiate EL emission at 524–540 nm, which is progressively red-shifted along with the increase of doping concentration. Device 3A shows the best EL performance among these doped devices, with $\eta_{C,max}$, $\eta_{P,max}$ and $\eta_{ext,max}$ values of 37.6 cd A^{-1}, 17.8 lm W^{-1} and 12.1%, respectively. Furthermore, the efficiency roll-off of Device 3A is considerably small with a value of 0.08% at the luminance of 1000 cd m^{-2}. Similar EL performances can also be observed in Devices 3B and 3C. These results indicate that both doped and nondoped devices based on these new emitters can achieve good EL performances with improved efficiency stability.

Since the film quality has a significant impact on the device performance, we tested the quality and morphology of the spin-coated films of both compounds by using atomic force microscopy (AFM). The films were prepared on silicon substrates according to the most efficient nondoped and doped devices by the same spin-coating method as that described for device fabrication. As illustrated in Fig. 8, the neat films of CC6-DBP-PXZ and CC6-DBP-DMAC show a smooth surface with small root mean square (RMS) values of 0.378 and 0.381 nm, respectively, indicating that they can form uniform films by the solution-processing technique. In addition, the doped films also have good quality, with small RMS values of 0.381 for 30 wt% CC6-DBP-DMAC:CBP and 0.390 nm for 10 wt% CC6-DBP-DMAC:CBP, which are similar to those of their neat films.

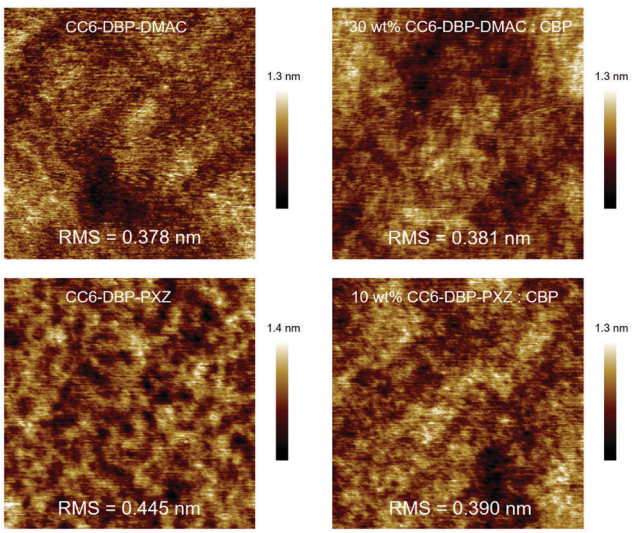

Fig. 8 AFM images of the neat and doped films of CC6-DBP-PXZ and CC6-DBP-DMAC. Neat films: Si/PEDOT:PSS (50 nm)/PVK (30 nm)/CC6-DBP-PXZ (40 nm); Si/PEDOT:PSS (50 nm)/PVK (30 nm)/CC6-DBP-DMAC (60 nm). Doped films: Si/PEDOT:PSS (50 nm)/PVK (30 nm)/10 wt% CC6-DBP-PXZ: CBP (50 nm); Si/PEDOT:PSS (50 nm)/PVK (30 nm)/30 wt% CC6-DBP-DMAC: CBP (55 nm).

Generally, solution-processed devices seriously suffer from the exciton quenching process, resulting in a considerably low efficiency and large efficiency roll-off. However, these new emitters with AIDF exhibit much better EL performance. More importantly, extremely small efficiency roll-offs are successfully achieved, which is a clear advance over conventional TADF emitters for solution-processed OLEDs. The high-concentration excitons at high voltages often give rise to severe exciton annihilation by bimolecular quenching processes (TTA, STA, *etc.*). These processes generally involve short-range Dexter energy transfer (DET) among molecules. In that case, the high-concentration exciton annihilation can be effectively reduced by elongating the distance between excitons. Concerning our compounds, it is considered that the excitons are mainly located at the central carbonyl groups because of the low energy level. Both compounds are highly twisted and adopt a loose packing in the aggregated state, which can protect excitons from getting close. Thus, the high-concentration exciton annihilation by the DET process can be suppressed to a large extent, leading to a greatly reduced efficiency roll-off.

Conclusions

In summary, two new luminescent small molecules comprising an electron-withdrawing benzoyl and electron-donating 9-hexylcarbazole and PXZ (or DMAC) moiety are designed and synthesized. They have high thermal and morphological stabilities and good electrochemical stability. Whereas they emit weakly without evident delayed fluorescence in the solution state, they turned out to be strong emitters with prominent delayed fluorescence in the aggregated state, demonstrating AIDF. In addition, they fluoresce intensely in spin-coated neat films with notable delayed fluorescence, owing to the small ΔE_{ST} and thus fast RISC process. As a consequence, they can perform excellently as light-emitting layers in solution-processed nondoped OLEDs, which exhibit a high $\eta_{ext,max}$ of 9.02% and negligible efficiency roll-off at the luminance of 1000 cd m^{-2}. On the other hand, both compounds also behave efficiently as dopants in a CBP host at varied doping concentrations of 10, 30 and 50 wt%, endowing the solution-processed doped OLEDs with a high $\eta_{ext,max}$ of up to 12.1%. More importantly, unlike most doped OLEDs based on TADF emitters, whose efficiency roll-off is quite serious, these solution-processed doped OLEDs present an extremely small efficiency roll-off of 0.08%, demonstrating their outstanding efficiency stability. The crucial factor for achieving high performance in devices is probably the AIDF character of the compounds, which combines the superior features of efficient solid-state emission, high exciton utilization and low exciton quenching. These results indicate the great potential of small molecules with AIDF for the fabrication of high-performance solution-processed OLEDs.

Experimental section

Synthesis and characterization

9-Hexylcarbazole (1). Potassium *tert*-butoxide (4.49 g, 40 mmol) was added to a mixture of carbazole (3.34 g, 20 mmol) and

1-bromohexane (4.21 mL, 30 mmol) in dehydrated tetrahydrofuran (100 mL) and stirred for 12 hours at room temperature. The reaction mixture was filtered, and the filtrate was concentrated and purified by column chromatography on silica gel (dichloromethane : petroleum ether, 1 : 10 v/v) to afford **1** as a white solid in 98% yield (4.93 g). ^{1}H NMR (500 MHz, $CDCl_3$) δ (ppm): 8.11–8.08 (m, 2H), 7.48–7.43 (m, 2H), 7.40 (d, J = 8.2 Hz, 2H), 7.25–7.20 (m, 2H), 4.29 (t, J = 7.3 Hz, 2H), 1.91–1.83 (m, 2H), 1.43–1.35 (m, 2H), 1.35–1.25 (m, 4H), 0.89–0.83 (m, 3H). ^{13}C NMR (125 MHz, $CDCl_3$) δ (ppm): 140.40, 125.53, 122.78, 120.31, 118.65, 108.62, 43.08, 31.59, 28.93, 26.98, 22.54, 14.01.

(9-Hexylcarbazole-3,6-diyl)bis((4-fluorophenyl)methanone) (3). Aluminum trichloride (1.28 g, 9.6 mmol) was added into a stirred solution of **1** (1.01 g, 4 mmol) and 4-fluorobenzoyl chloride (**2**) (1.90 g, 12.0 mmol, 1.42 mL) in dehydrated dichloromethane (50 mL) in an ice bath and left stirring for 15 min. Then, the reaction mixture was warmed back to room temperature and stirred for 3 h. The reaction was quenched with ice water and hydrochloric acid (50 mL, 2 : 1 v/v), and extracted with dichloromethane several times. The combined organic layers were washed with water twice, and then dried over anhydrous $MgSO_4$. After filtration and solvent evaporation under reduced pressure, the residue was purified by column chromatography on silica gel (dichloromethane : petroleum ether, 2 : 1 v/v) to afford **3** as a white solid in 96% yield (1.90 g). ^{1}H NMR (500 MHz, $CDCl_3$) δ (ppm): 8.56 (d, J = 1.3 Hz, 2H), 8.07–8.02 (m, 2H), 7.90–7.85 (m, 4H), 7.52 (d, J = 8.6 Hz, 2H), 7.23–7.17 (m, 4H), 4.40 (t, J = 7.3 Hz, 2H), 1.98–1.90 (m, 2H), 1.45–1.39 (m, 2H), 1.38–1.27 (m, 4H), 0.91–0.85 (m, 3H). ^{13}C NMR (125 MHz, $CDCl_3$) δ (ppm): 195.02, 166.14, 164.13, 143.73, 134.78, 134.76, 132.52, 132.45, 129.52, 128.97, 123.92, 122.69, 115.55, 115.38, 109.04, 43.72, 31.50, 28.95, 26.91, 22.52, 13.99.

((9-Hexylcarbazole-3,6-diyl)bis((4-(phenoxazin-10-yl)phenyl)-methanone)) (CC6-DBP-PXZ). A mixture of **3** (0.99 g, 2 mmol) and phenoxazine (**4a**) (1.10 g, 6 mmol) in deaerated and dehydrated *N*,*N*-dimethylformamide (20 mL) was stirred for 15 min under argon at room temperature, and then the reaction mixture was heated up to 110 °C and potassium *tert*-butoxide (0.45 g, 4 mmol) was added and stirred for 12 h. After cooling down to room temperature, the reaction was quenched with water (20 mL) and extracted with dichloromethane several times. The combined organic layers were washed with water twice, and then dried over anhydrous $MgSO_4$. After filtration and solvent evaporation under reduced pressure, the residue was purified by column chromatography on silica gel (dichloromethane : petroleum ether, 3 : 1 v/v) to afford an orange solid of CC6-DBP-PXZ in 45% yield (0.74 g). ^{1}H NMR (500 MHz, $CDCl_3$) δ (ppm): 8.78 (d, J = 1.4 Hz, 2H), 8.13–8.07 (m, 6H), 7.57 (d, J = 8.6 Hz, 2H), 7.53 (d, J = 8.4 Hz, 4H), 6.78–6.61 (m, 12H), 6.05 (d, J = 7.9 Hz, 4H), 4.48–4.39 (m, 2H), 2.01–1.92 (m, 2H), 1.48–1.42 (m, 2H), 1.40–1.29 (m, 4H), 0.90–0.87 (m, 3H). ^{13}C NMR (125 MHz, $CDCl_3$) δ 195.33, 144.03, 143.95, 142.65, 138.42, 133.83, 132.73, 130.83, 129.36, 129.29, 123.93, 123.35, 122.98, 121.79, 115.67, 113.43, 109.01, 53.43, 43.79, 31.51, 28.95, 26.93, 22.52, 13.99. HRMS ($C_{56}H_{43}N_3O_4$): m/z 821.3274 [M^+, calcd 821.3254].

(9-Hexylcarbazole-3,6-diyl)bis((4-(9,9-dimethylacridin-10-yl)-phenyl)methanone) (CC6-DBP-DMAC). The procedure was analogous to that described for CC6-DBP-PXZ. A yellow solid of CC6-DBP-DMAC was obtained in 32% yield. ^{1}H NMR (500 MHz, $CDCl_3$) δ (ppm): 8.83 (d, J = 1.4 Hz, 2H), 8.17–8.10 (m, 6H), 7.58 (d, J = 8.6 Hz, 2H), 7.55–7.51 (m, 4H), 7.50–7.46 (m, 4H), 7.05–7.00 (m, 4H), 7.00–6.94 (m, 4H), 6.44–6.35 (m, 4H), 4.50–4.39 (m, 2H), 2.01–1.94 (m, 2H), 1.71 (s, 12H), 1.49–1.43 (m, 2H), 1.39–1.30 (m, 4H), 0.91–0.87 (m, 3H). ^{13}C NMR (125 MHz, $CDCl_3$) δ (ppm): 195.54, 145.00, 143.92, 140.55, 138.04, 132.62, 131.01, 130.55, 129.45, 129.39, 126.48, 125.31, 123.93, 123.01, 121.05, 114.38, 108.95, 43.78, 36.08, 31.51, 31.10, 28.96, 26.94, 22.52, 14.00. HRMS ($C_{62}H_{55}N_3O_2$): m/z 859.4166 [$(M–CH_3)^+$, calcd 859.4138].

X-ray crystallography

Crystal data for CC6-DBP-PXZ (CCDC 1838714): $C_{56}H_{43}N_3O_4 \cdot 0.64CH_2Cl_2 \cdot 0.36CH_3OH$, M_W = 888.04, monoclinic, $P21/c$, a = 7.1750(6), b = 18.3221(16), c = 33.824(3) Å, β = 91.414(2)°, V = 4445.2(6) Å^3, Z = 4, D_c = 1.327 g cm^{-3}, μ = 0.158 mm^{-1} (MoKα, λ = 0.71073), $F(000)$ = 1862, T = 173(2) K, $2\theta_{max}$ = 25.02° (98.8%), 24 697 measured reflections, 7776 independent reflections (R_{int} = 0.1029), GOF on F^2 = 1.036, R_1 = 0.1540, wR_2 = 0.1488 (all data), Δe 0.345 and −0.362 e Å^{-3}.

Device fabrication and measurement

The devices were fabricated on clean glass substrates pre-coated with an indium tin oxide (ITO) layer (180 nm) with a sheet resistance of 10 Ω per square. The ITO surface was treated in an ultrasonic detergent bath for 90 min, followed by soaking in ultrasonic de-ionized water for 20 min, then drying at 120 °C for 1 h, and UV/Ozone cleaning for 15 min before spin coating. A PEDOT:PSS layer (50 nm) was spin-coated onto the ITO surface at 3000 rpm, then baked at 150 °C for 15 min to remove the residual water. Then, the substrates were moved into a glovebox with a N_2 atmosphere, and a PVK layer was spin-coated onto the PEDOT:PSS layer at 2000 and 2500 rpm (the thickness achieved was 35 and 30 nm, respectively) from a filtered 10 mg mL^{-1} chlorobenzene solution, followed by drying at 120 °C for 20 min. Then, the emitting layer was spin-coated according to the configuration requirement. Here, CC6-DBP-DMAC and CC6-DBP-PXZ were dissolved in chlorobenzene with a concentration of 20 mg mL^{-1}. Nondoped CC6-DBP-DMAC or CC6-DBP-PXZ layers were spin-coated at 1500, 2000, and 3500 rpm for 45 s to get a thickness of 65, 60, and 40 nm, respectively. Solutions of CC6-DBP-DMAC or CC6-DBP-PXZ (10, 30 and 50 wt%) doped in CBP with an overall concentration of 20 mg mL^{-1} in chlorobenzene were spin-coated at 2000 rpm for 45 s to get films with a thickness of 50, 55 and 60 nm, respectively. Finally, an electron-transport layer TmPyPB, a LiF layer, and an Al layer were deposited consecutively onto the spin-coated film in a vacuum chamber at 10^{-4} Pa. The emission area of the device was 4 × 4 mm^{-2}, as shaped by the overlapping area of the anode and cathode. All the device characterization steps were carried out at room temperature under ambient laboratory conditions without encapsulation except

the spectrum collection process. EL spectra were recorded by an optical analyzer, FlAME-S-VIS-NIR. Current density and luminance *versus* driving voltage characteristics were measured by a Keithley 2400 and a Konica Minolta chromameter CS-200. External quantum efficiencies were calculated by assuming that the devices were Lambertian light sources.

Conflicts of interest

There are no conflicts of interest to declare.

Acknowledgements

This work was financially supported by the National Natural Science Foundation of China (21788102 and 21673082), the National Key Basic Research and Development Program of China (973 program, 2015CB655004) Founded by MOST, the Guangdong Natural Science Funds for Distinguished Young Scholar (2014A030306035), the Natural Science Foundation of Guangdong Province (2016A030312002), the Science and Technology Project of Guangdong Province (2016B090907001), the Science and Technology Program of Guangzhou (201804020027 and 201704030069), the Innovation and Technology Commission of Hong Kong (ITC-CNERC14SC01) and the Fundamental Research Funds for the Central Universities (2017ZD001).

References

1 (*a*) H. Uoyama, K. Goushi, K. Shizu, H. Nakamura and C. Adachi, *Nature*, 2012, **492**, 234; (*b*) Q. Zhang, J. Li, K. Shizu, S. Huang, S. Hirata, H. Miyazaki and C. Adachi, *J. Am. Chem. Soc.*, 2012, **134**, 14706; (*c*) S. Hirata, Y. Sakai, K. Masui, H. Tanaka, S. Y. Lee, H. Nomura, N. Nakamura, M. Yasumatsu, H. Nakanotani, Q. Zhang, K. Shizu, H. Miyazaki and C. Adachi, *Nat. Mater.*, 2015, **14**, 330.

2 (*a*) Q. Wei, N. Fei, A. Islam, T. Lei, L. Hong, R. Peng, X. Fan, L. Chen, P. Gao and Z. Ge, *Adv. Opt. Mater.*, 2018, **6**, 1800512; (*b*) B. Wex and B. R. Kaafarani, *J. Mater. Chem. C*, 2017, **5**, 8622; (*c*) M. Godumala, S. Choi, M. J. Cho and D. H. Choi, *J. Mater. Chem. C*, 2016, **4**, 11355; (*d*) Z. Yang, Z. Mao, Z. Xie, Y. Zhang, S. Liu, J. Zhao, J. Xu, Z. Chi and M. P. Aldred, *Chem. Soc. Rev.*, 2017, **46**, 915; (*e*) M. Y. Wong and E. Zysman-Colman, *Adv. Mater.*, 2017, **29**, 1605444; (*f*) X. Cao, D. Zhang, S. Zhang, Y. Tao and W. Huang, *J. Mater. Chem. C*, 2017, **5**, 7699; (*g*) D. Zhang, X. Song, M. Cai, H. Kaji and L. Duan, *Adv. Mater.*, 2018, **30**, 1705406; (*h*) J. H. Kim, J. H. Yun and J. Y. Lee, *Adv. Opt. Mater.*, 2018, **6**, 1800255.

3 (*a*) P. Rajamalli, N. Senthilkumar, P. Gandeepan, P.-Y. Huang, M.-J. Huang, C.-Z. Ren-Wu, C.-Y. Yang, M.-J. Chiu, L.-K. Chu, H.-W. Lin and C.-H. Cheng, *J. Am. Chem. Soc.*, 2016, **138**, 628; (*b*) P. Rajamalli, N. Senthilkumar, P.-Y. Huang, C.-C. Ren-Wu, H.-W. Lin and C.-H. Cheng, *J. Am. Chem. Soc.*, 2017, **139**, 10948; (*c*) G. Xie, J. Luo, M. Huang, T. Chen, K. Wu, S. Gong and C. Yang, *Adv. Mater.*, 2017, **29**, 1604223; (*d*) X. Cai, X. Li, G. Xie, Z. He, K. Gao, K. Liu, D. Chen, Y. Cao and S.-J. Su, *Chem. Sci.*, 2016, **7**, 4264.

4 (*a*) D. Zhang, P. Wei, D. Zhang and L. Duan, *ACS Appl. Mater. Interfaces*, 2017, **9**, 19040; (*b*) F. B. Dias, J. Santos, D. R. Graves, P. Data, R. S. Nobuyasu, M. A. Fox, A. S. Batsanov, T. Palmeira, M. N. Berberan-Santos, M. R. Bryce and A. P. Monkman, *Adv. Sci.*, 2016, **3**, 1600080; (*c*) P. L. dos Santos, J. S. Ward, M. R. Bryce and A. P. Monkman, *J. Phys. Chem. Lett.*, 2016, **7**, 3341; (*d*) J.-A. Seo, Y. Im, S. H. Han, C. W. Lee and J. Y. Lee, *ACS Appl. Mater. Interfaces*, 2017, **9**, 37864; (*e*) C. Li, R. Duan, B. Liang, G. Han, S. Wang, K. Ye, Y. Liu, Y. Yi and Y. Wang, *Angew. Chem., Int. Ed.*, 2017, **56**, 11525; (*f*) Y. Yuan, Y. Hu, Y.-X. Zhang, J.-D. Lin, Y.-K. Wang, Z.-Q. Jiang, L.-S. Liao and S.-T. Lee, *Adv. Funct. Mater.*, 2017, **27**, 1700986.

5 (*a*) R. J. Holmes, S. R. Forrest, Y. J. Tung, R. C. Kwong, J. J. Brown, S. Garon and M. E. Thompson, *Appl. Phys. Lett.*, 2003, **82**, 2422; (*b*) X. Gong, J. C. Ostrowski, D. Moses, G. C. Bazan and A. J. Heeger, *Adv. Funct. Mater.*, 2003, **13**, 439.

6 (*a*) J. Guo, Z. Zhao and B. Z. Tang, *Adv. Opt. Mater.*, 2018, **6**, 1800264; (*b*) H. Liu, J. Zeng, J. Guo, H. Nie, Z. Zhao and B. Z. Tang, *Angew. Chem., Int. Ed.*, 2018, **57**, 9290; (*c*) J. Huang, H. Nie, J. Zeng, Z. Zhuang, S. Gan, Y. Cai, J. Guo, Z. Zhao and B. Z. Tang, *Angew. Chem., Int. Ed.*, 2017, **56**, 12971; (*d*) J. Guo, X.-L. Li, H. Nie, W. Luo, S. Gan, S. Hu, R. Hu, A. Qin, Z. Zhao, S.-J. Su and B. Z. Tang, *Adv. Funct. Mater.*, 2017, **27**, 1606458; (*e*) J. Guo, X.-L. Li, H. Nie, W. Luo, R. Hu, A. Qin, Z. Zhao, S.-J. Su and B. Z. Tang, *Chem. Mater.*, 2017, **29**, 3623; (*f*) S. Gan, J. Zhou, T. A. Smith, H. Su, W. Luo, Y. Hong, Z. Zhao and B. Z. Tang, *Mater. Chem. Front.*, 2017, **1**, 2554.

7 (*a*) R. Furue, T. Nishimoto, I. S. Park, J. Lee and T. Yasuda, *Angew. Chem., Int. Ed.*, 2016, **55**, 7171; (*b*) N. Aizawa, C.-J. Tsou, I. S. Park and T. Yasuda, *Polym. J.*, 2017, **49**, 197; (*c*) S. Y. Park, S. Choi, G. E. Park, H. J. Kim, C. Lee, J. S. Moon, S. W. Kim, S. Park, J. H. Kwon, M. J. Cho and D. H. Choi, *ACS Appl. Mater. Interfaces*, 2018, **10**, 14966; (*d*) H. Zhao, Z. Wang, X. Cai, K. Liu, Z. He, X. Liu, Y. Cao and S.-J. Su, *Mater. Chem. Front.*, 2017, **1**, 2039.

8 H. Wu, L. Ying, W. Yang and Y. Cao, *Chem. Soc. Rev.*, 2009, **38**, 3391.

9 (*a*) S. Shao, J. Hu, X. Wang, L. Wang, X. Jing and F. Wang, *J. Am. Chem. Soc.*, 2017, **139**, 17739; (*b*) S. Y. Lee, T. Yasuda, H. Komiyama, J. Lee and C. Adachi, *Adv. Mater.*, 2016, **28**, 4019; (*c*) Z. Ren, R. S. Nobuyasu, F. B. Dias, A. P. Monkman, S. Yan and M. R. Bryce, *Macromolecules*, 2016, **49**, 5452; (*d*) Y. Wang, Y. Zhu, X. Lin, Y. Yang, B. Zhang, H. Zhan, Z. Xie and Y. Cheng, *J. Mater. Chem. C*, 2018, **6**, 568.

10 (*a*) H. J. Kim, C. Lee, M. Godumala, S. Choi, S. Y. Park, M. J. Cho, S. Park and D. H. Choi, *Polym. Chem.*, 2018, **9**, 1318; (*b*) Y. Hu, W. Cai, L. Ying, D. Chen, X. Yang, X.-F. Jiang, S. Su, F. Huang and Y. Cao, *J. Mater. Chem. C*, 2018, **6**, 2690; (*c*) X. Zeng, J. Luo, T. Zhou, T. Chen, X. Zhou, K. Wu, Y. Zou, G. Xie, S. Gong and C. Yang, *Macromolecules*, 2018, **51**, 1; (*d*) P. Pander, S. Gogoc, M. Colella, P. Data and F. B. Dias, *ACS Appl. Mater. Interfaces*, 2018, **10**, 28796.

11 (*a*) Z. Zhao, J.-H. Li, X. Chen, P. Lu and Y. Yang, *Org. Lett.*, 2008, **10**, 3041; (*b*) Z. Zhao, J.-H. Li, P. Lu and Y. Yang, *Adv. Funct. Mater.*, 2007, **17**, 2203.

12 (*a*) X. Yang, H. Guo, B. Liu, J. Zhao, G. Zhou, Z. Wu and W.-Y. Wong, *Adv. Sci.*, 2018, **5**, 1701067; (*b*) C.-H. Lee, M.-C. Tang, W.-L. Cheung, S.-L. Lai, M.-Y. Chan and V. W.-W. Yam, *Chem. Sci.*, 2018, **9**, 6228; (*c*) Y. Li, G. Xie, S. Gong, K. Wu and C. Yang, *Chem. Sci.*, 2016, **7**, 5441.

13 (*a*) M. Godumala, S. Choi, H. J. Kim, C. Lee, S. Park, J. S. Moon, K. S. Woo, J. H. Kwon, M. J. Cho and D. H. Choi, *J. Mater. Chem. C*, 2018, **6**, 1160; (*b*) X. Liao, X. Yang, R. Zhang, J. Cheng, J. Li, S. Chen, J. Zhu and L. Li, *J. Mater. Chem. C*, 2017, **5**, 10001; (*c*) K. Matsuoka, K. Albrecht, A. Nakayama, K. Yamamoto and K. Fujita, *ACS Appl. Mater. Interfaces*, 2018, **10**, 33343; (*d*) K. Wu, Z. Wang, L. Zhan, C. Zhong, S. Gong, G. Xie and C. Yang, *J. Phys. Chem. Lett.*, 2018, **9**, 1547; (*e*) X. Liao, X. Yang, J. Cheng, Y. Li, X. Meng, J. Li, Q. Pei and L. Li, *ChemPlusChem*, 2018, **83**, 274; (*f*) G. Xie, X. Li, D. Chen, Z. Wang, X. Cai, D. Chen, Y. Li, K. Liu, Y. Cao and S.-J. Su, *Adv. Mater.*, 2016, **28**, 181; (*g*) T. Huang, W. Jiang and L. Duan, *J. Mater. Chem. C*, 2018, **21**, 5577; (*h*) Y. Zou, S. Gong, G. Xie and C. Yang, *Adv. Opt. Mater.*, 2018, 1800568.

14 (*a*) Y. Wada, S. Kubo and H. Kaji, *Adv. Mater.*, 2018, **30**, 1705641; (*b*) K. Sun, Y. Sun, W. Tian, D. Liu, Y. Feng, Y. Sun and W. Jiang, *J. Mater. Chem. C*, 2018, **6**, 43; (*c*) Y. J. Cho, B. D. Chin, S. K. Jeon and J. Y. Lee, *Adv. Funct. Mater.*, 2015, **25**, 6786; (*d*) X. Li, K. Wang, Y.-Z. Shi, M. Zhang, G.-L. Dai, W. Liu, C.-J. Zheng, X.-M. Ou and X.-H. Zhang, *J. Mater. Chem. C*, 2018, **6**, 9152; (*e*) K. Albrecht, K. Matsuoka, K. Fujita and K. Yamamoto, *Angew. Chem., Int. Ed.*, 2015, **54**, 5677; (*f*) X. Ban, F. Chen, Y. Zhao, A. Zhu, Z. Tong, W. Jiang and Y. Sun, *ACS Appl. Mater. Interfaces*, 2018, **10**, 37335; (*g*) K. Matsuoka, K. Albrecht, A. Nakayama, K. Yamamoto and K. Fujita, *ACS Appl. Mater. Interfaces*, 2018, **10**, 33343.

15 (*a*) Z. Zhao, P. Lu, J. W. Y. Lam, Z. Wang, C. Y. K. Chan, H. H. Y. Sung, I. D. Williams, Y. Ma and B. Z. Tang, *Chem. Sci.*, 2011, **2**, 672; (*b*) Z. Zhao, S. Chen, J. W. Y. Lam, Z. Wang, P. Lu, F. Mahtab, H. H. Y. Sung, I. D. Williams, Y. Ma, H. S. Kwok and B. Z. Tang, *J. Mater. Chem.*, 2011, **21**, 7210; (*c*) Y. Zhang, B. He, J. Liu, L. Pan, Z. Zhao and B. Z. Tang, *Phys. Chem. Chem. Phys.*, 2018, **20**, 9922.

16 (*a*) Q. Li and Z. Li, *Adv. Sci.*, 2017, **4**, 1600484; (*b*) Z. Zhao, B. He and B. Z. Tang, *Chem. Sci.*, 2015, **6**, 5347; (*c*) P. Shen, Z. Zhuang, Z. Zhao and B. Z. Tang, *J. Mater. Chem. C*, 2018, **6**, 11835; (*d*) J. Mei, Y. Hong, J. W. Y. Lam, A. Qin, Y. Tang and B. Z. Tang, *Adv. Mater.*, 2014, **26**, 5429; (*e*) J. Mei, N. L. C. Leung, R. T. K. Kwok, J. W. Y. Lam and B. Z. Tang, *Chem. Rev.*, 2015, **115**, 11718.

17 (*a*) J. Fan, L. Lin and C.-K. Wang, *J. Mater. Chem. C*, 2017, **5**, 8390; (*b*) J. Fan, Y. Zhang, Y. Zhou, L. Lin and C.-K. Wang, *J. Phys. Chem. C*, 2018, **122**, 2358.

18 C. M. Cardona, W. Li, A. E. Kaifer, D. Stockdale and G. C. Bazan, *Adv. Mater.*, 2011, **23**, 2367.